

Investigation of Microstructure Properties and Quantitative Metallography by Different Etchants in the Service-Exposed Nickel-Based Superalloy Turbine Blade

Amirhossein Khodabakhshi¹ · Alireza Mashreghi¹ · Yazdan Shajari² · Seyed Hossein Razavi³

Received: 24 February 2017 / Accepted: 20 October 2017 / Published online: 20 November 2017
© The Indian Institute of Metals - IIM 2017

Abstract In this study, the effect of etchant type and etching conditions on the root and airfoil microstructure of a service-exposed IN738 turbine blade has been investigated. The microstructure of superalloy components used at high temperatures, in addition to the usual microstructural changes, experiences deterioration in micrometer dimensions. In order to investigate these changes, electrochemical etching was performed on the samples with the chemical solution including 80% phosphoric acid, solution containing Cr₂O₃ and 55% glycerol. Chemical etching was performed with marble and etchant solution containing 60% glycerol. The results in terms of specifying the deterioration effects on microstructure of the blade applied at high temperature, the amount of γ' phase and the best etchant were investigated. Among the solutions used for chemical etching, the solution containing 10 ml HNO₃, 50 ml HCl and 60 ml glycerol was appropriate for detection of segregations and dendrites, and among the electrochemical etching solutions, the Cr₂O₃ solution was found suitable for specifying γ' precipitates' morphology by scanning electron microscopy. In this research, the results of the quantitative analysis of the images provided by these etchants were also investigated.

Keywords Nickel-based superalloy · Microstructure · Chemical etching · Electro-etch

1 Introduction

Nickel base superalloys are a group of metal alloys with an exceptional combination of high temperature resistance, toughness, and corrosion resistance. These materials are used widely in power plant turbines, aircraft engines, rocket engines and other special environments such as nuclear plants [1–4]. Nowadays, superalloys in terms of economic issues and creep behavior have special applications. Normally, gas turbine blades used in power generation plants work at high temperatures and high stresses. The first stage blades of these turbines are usually made of nickel-based superalloys especially IN738-LC superalloy [5]. The main element of this superalloy is nickel which constitutes more than 50 wt.% of the alloy and about 10 other elements are added to it. The Ni–Al–Ti Triple system is a main alloying system in superalloys. With the addition of Al and Ti in the alloy matrix, the precipitation γ' phase is constructed with the chemical composition of Ni₃ (Al, Ti). The mechanical properties of nickel-based superalloys highly depend on the volume percent, distribution and morphology of γ' precipitates and on the cooling rates higher than 40 °C/min. A uniform distribution of fine γ' precipitates is obtained during the partial solution heat treatment. Lower cooling rates cause the production of γ' precipitates with relatively large size [6, 7]. In addition, the presence of a specific set of alloying elements in precipitation hardening nickel-based superalloys leads to the production of γ matrix, MC and M₂₃C₆ complex carbides and γ – γ' eutectic phases [7, 8].

✉ Yazdan Shajari
yazdan.shajari@yahoo.com

¹ Department of Mining and Metallurgical Engineering, Yazd University, Yazd, Iran

² Department of Materials Engineering, Islamic Azad University, Karaj Branch, Karaj, Iran

³ School of Metallurgy and Materials Engineering, Iran University of Science and Technology (IUST), Tehran, Iran

Microstructural and mechanical properties changes occur in the blades made of these superalloys after a period of working at high temperatures due to phenomena such as diffusion, creep, hot corrosion and oxidation; these changes are often accompanied by loss of mechanical properties. It has been reported that with the exposure of IN738-LC alloy to high temperature and stress during service for a long time, γ' fine particles interrelate and constitute the coarser particles and also the morphology of the particles changes from cubic to spherical shape [9, 10]. Another issue that occurs in working conditions of superalloys is MC carbide decomposition [11, 12]. This instability in the microstructure reduces creep strength at elevated temperatures [5, 13]. MC carbide is usually large and blocky shaped and it can be seen within the grains and grain boundaries [14–16]. $M_{23}C_6$ carbide tends to be in the grain boundaries and it has frequently been observed as discontinuous and irregular block parts. In order to detect the microstructural changes in the superalloys, extensive studies have been conducted on the morphology and amount of γ' precipitates in different ways. The detection of microstructure of nickel based superalloys that has been under heat-treated or high-temperature service-exposed is a very detailed process and sometimes with errors due to the various alloying elements, different phases and continuous permutations that occur during service period. The etch method and the type of used etchant are two important parameters that have a great influence on the quality of the images and observable phases. The main purpose in this research is the manner to portray the microstructural changes created in used blade of IN738-LC by different etchants. In this study, the microstructure of the airfoil and the root of a plant turbine blade that had undergone undesirable changes due to long time use, have been investigated by different etchants.

2 Experimental

The samples used in this study were provided by a piece of used turbine. The mentioned blade was out of service due to the long term operation. The results of chemical analysis of the blade are given in Table 1. A Comparison of the weight percent of standard amounts showed that the used alloy in terms of chemical composition corresponded with the allowed range of IN738-LC superalloy elements. The studied samples with the same dimensions were separated by wire discharge cutting. In addition to the airfoil, samples for microstructural comparison were also provided from root part. The γ' precipitates are the most important and influential phase on the mechanical properties and have the greatest influence towards thermal treatment. Therefore, a method and etchant were considered for appropriate detection in order to demonstrate γ' precipitates in high resolution. So, at first the samples were mounted and then were ground through successive grades of silicon carbide abrasive papers (SiC grit papers) from P100 to P2000 mesh according to common grinding procedures. Polishing was performed using cloth disc and 0.3 μm alumina suspension. After preparation of the sample, to study the effect of different etchants on revealed microstructure features specially deterioration in microstructure, the samples were etched by different etchants. The used etchant and etching conditions for each sample is given in Table 2. Microstructure of the samples were investigated by means of a CX51 Olympus optical microscope (OM), Tescan vega3 scanning electron microscopy (SEM) and Tescan mira3 field emission scanning electron microscopy (FESEM) equipped with energy dispersive X-ray (EDX) microanalysis hardware. Also volume fraction and Average diameter of the primary γ' in airfoil microstructure was calculated by using the image analysis software, Image J

Table 1 Chemical composition of the alloy IN738LC used in this study (wt.%)

Chemical element	C	Cr	Mo	Co	Ni	Ta	W	Al	Ti	Zr	B	Fe
Composition	0.09	15.4	1.5	8.5	Base	2.3	2.9	3.2	3.2	0.05	0.01	0.1

Table 2 Etchants and etching methods used in this study

Etchant	Etchant solution	Etching method
No. 1	10 ml HCl, 50 ml CuSO_4 , 50 ml H_2O	Immersion etching for 10–15 s
No. 2	10 ml HNO_3 , 50 ml HCl, 60 ml glycerol	Immersion etching at 60 °C for 100–120 s
No. 3	37 ml H_3PO_4 , 56 ml glycerol, 7 ml H_2O	Electro etching, 4–6 V for 8 s
No. 4	12 ml H_3PO_4 , 47 ml H_2SO_4 , 41 ml HNO_3	Electro etching, 4 V for 6 s
No. 5	170 ml H_3PO_4 , 10 ml H_2SO_4 , 16 ml grCrO_3	Electro etching, 4–6 V for 4 s
No. 6	80 ml H_3PO_4 + 10 ml H_2O	Electro etching, 4 V for 8 s

and Image Pro-Plus, to compare the effect of different etchants on quantitative metallography.

3 Results and Discussion

3.1 Study of the Root Microstructure

Figure 1 shows the optical microscopy image of the microstructure related to the root section provided by different etchant (Table 2). The microstructure consists of large grains with an average diameter of about 220 μm . In Fig. 1a, b, which are provided by etchants No. 1 and No. 2,

dendritic arms with inter dendritic segregations (dark and light areas), as well as dispersed carbides (dark dots) can be observed clearly. Figure 1c, d show optical microscopy images provided by electro etching process related to etchants No. 3 and No. 4, respectively. This type of microstructure is similar to the images shown in Fig. 1a, b, while in Fig. 1a, b, dendritic arms have greater clarity and inter dendritic segregation can be observed with more contrast due to the different corrosion mechanisms of corresponding etchants.

The study of etchant No. 5 shows that the main corrosion mechanism for this etchant is also similar to No. 3 and No. 4 etchants. The optical images with higher magnification in

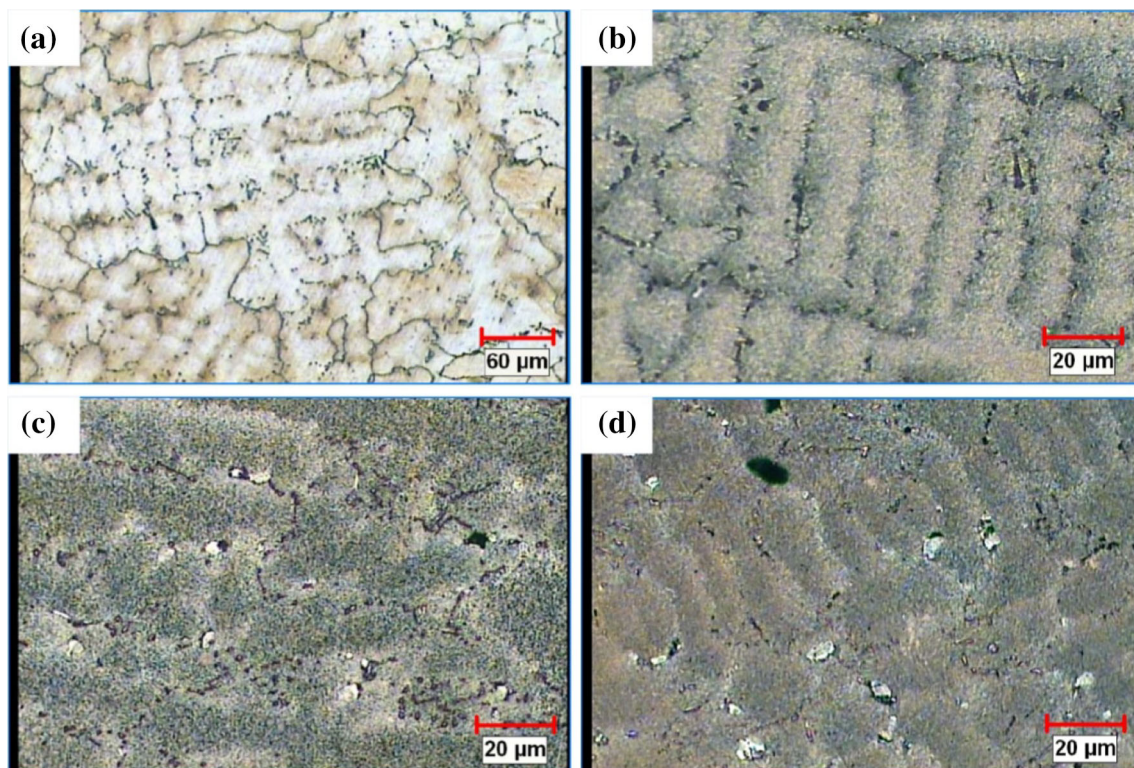
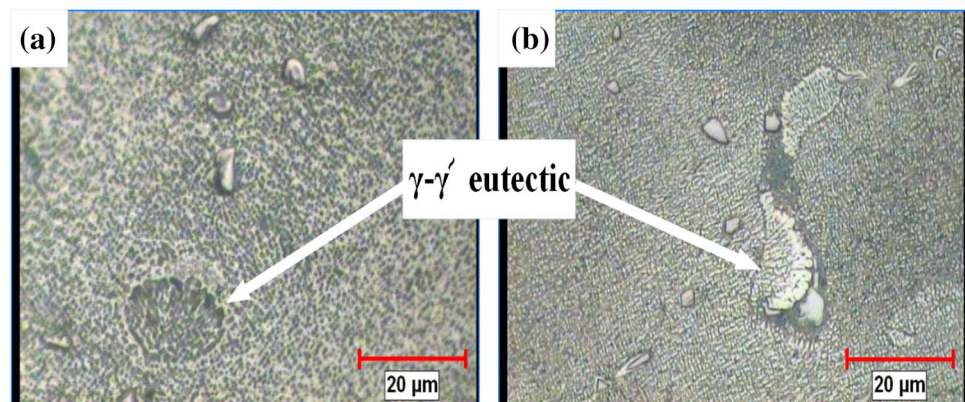


Fig. 1 Optical micrographs of the root samples etched by etchant **a** No. 1, **b** No. 2, **c** No. 3, **d** No. 4

Fig. 2 Optical micrographs of the root samples etched by etchant **a** No. 2, **b** No. 3



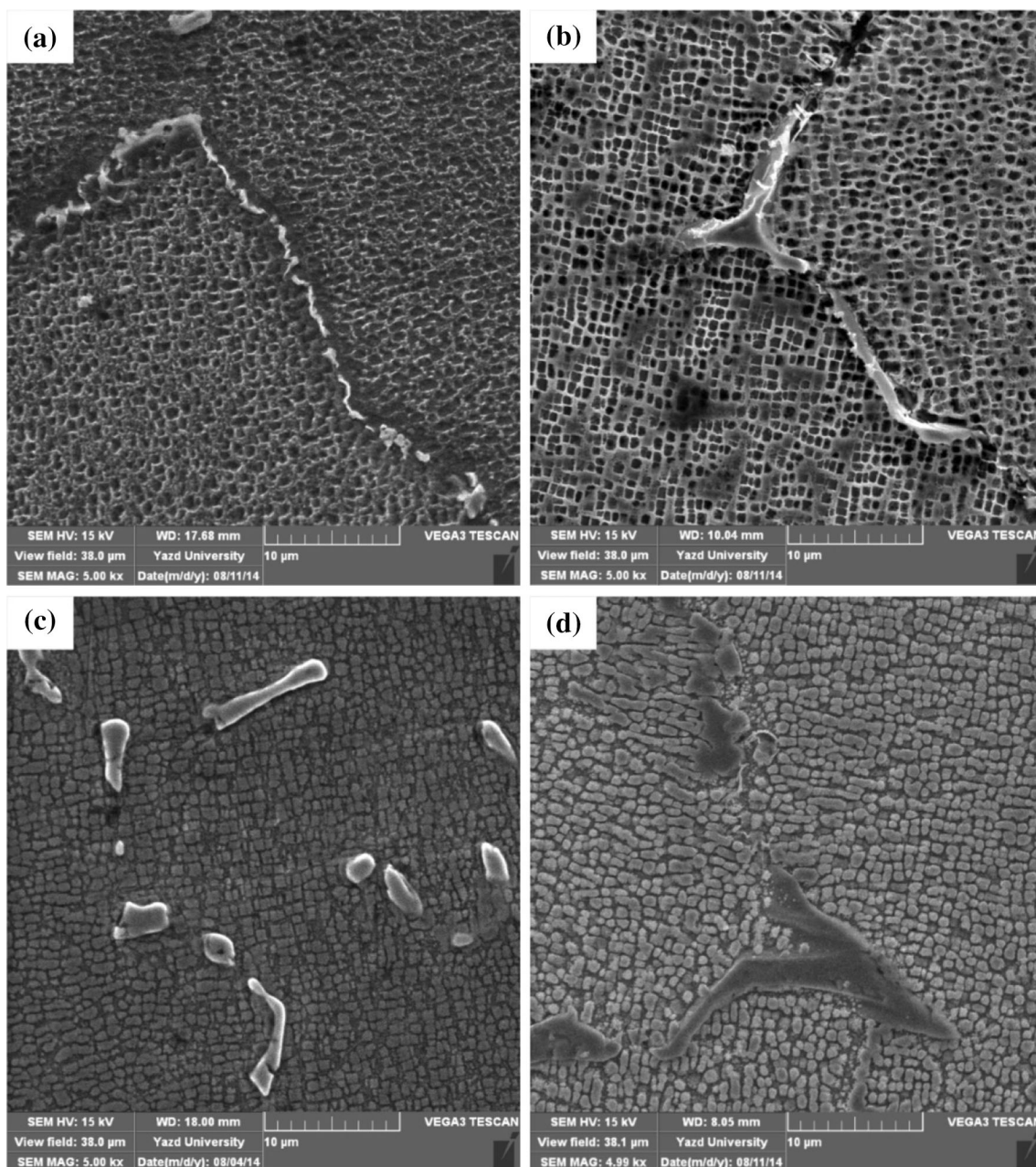


Fig. 3 SEM micrographs of MC and $M_{23}C_6$ carbides of the root samples etched by etchant **a** No. 1, **b** No. 2, **c** No. 3, **d** No. 5

Fig. 2 reveal more details of the etching mechanisms of different etchants used in this study. Figure 2a, b show eutectic γ - γ' phase. In Fig. 2a, it can be observed that the etchant No. 2 causes γ' eutectic phase corrosion; while Fig. 2b shows that in the sample etched by etchant No. 3, γ' phase is intact in the eutectic areas but the γ matrix has corroded, although the accurate recognition of the corrosion mechanism of each etchant needs use of electron microscopy images. The microstructure investigation of the images provided by etchants No. 4 and No. 5 also shows the results similar to etchant No. 2. In addition to the eutectic areas, the presence of MC carbides can be seen in Fig. 2.

The SEM images of MC and $M_{32}C_6$ carbides have been shown in Fig. 3. Figure 3a, b, d show $M_{23}C_6$ carbides precipitated on the grain boundaries and Fig. 3c shows microstructure of MC carbides. During the working period, MC carbides decompose slowly and convert to $M_{23}C_6$ carbides [17, 18]. The creation of the grain boundary carbides, especially $M_{23}C_6$, increases the grain boundary strength. The carbides prevent moving and joining of creep cavities during service period at high temperatures and decrease the grain boundary sliding [10]. The SEM studies reveal that etchants No.1 and 2 are γ' phase corrosive etchants (Fig. 3a, b) and etchants No. 3 and No. 5 cause

corrosion of the γ matrix phase (Fig. 3c, d). Generally, in order to determine the deterioration effects occurring in the root section microstructure, the morphology of MC and $M_{23}C_6$ carbides and γ' precipitates should be considered. The role of different etchants in revealing γ' microstructure and demonstrating the morphological changes caused by working at high temperatures, is very critical. In Fig. 4, γ' precipitates can be observed with regular distribution, the mean size of 750 nm and the volume fraction of 60% in the microstructure of the root. The images of Fig. 4 show the root microstructure at higher magnifications provided by different etchants. The growth of primary and secondary γ' particles can be observed in this image. This phenomenon occurs due to joining of secondary γ' particles to each other and becoming coarser particles as well as γ' initial growth due to joining of secondary γ' precipitates to them. Some signs of this phenomenon are seen in the images of Fig. 4 especially in Fig. 4d, e.

The microstructure of the root is presented in Fig. 5. This figure shows firstly, in addition to deformation of γ' precipitates, in some areas of the root there is continuous film on grain boundary due to precipitation of γ' phase at grain boundaries. Secondly, the accession process of the secondary precipitates to each other is being done. Thirdly, initial γ' precipitates are transshipping due to joining of secondary γ' . In Fig. 5-a, it can be observed that fine precipitates of the secondary γ' are joining to the grain boundaries and with more passage of time, thickening of the grain boundaries cause. It should be noted that γ' precipitation on grain boundaries cause the continuous film on grain boundaries and this is another factor for reduction of failure lifetime [19]. The comparison of Fig. 3a, b with Fig. 5a, b shows that in the chemical etch, the continuous film on grain boundaries cannot be specified due to corrosion in γ' phase. Although, in many of the literatures and conducted studies by researchers such as [20, 21], the microscopic structure of the root has been introduced as an original microstructure or in other words, the representative of the initial microstructure of the blade before operation, but effects of deterioration can be observed in the root microstructure in this study.

Etchants No. 1 and No. 2 have been selected as the most appropriate corrosive etchants of γ' phase respectively, and etchants No. 5 and No. 6 have been selected as the most appropriate corrosive etchants of matrix phase respectively, for the quality and clarity of the images provided in this investigation. SEM images of samples etched by these etchants have been used for quantitative investigation. Table 3 shows the volume fraction of γ' precipitate obtained by quantitative metallography. These samples have been extracted from the root section and their microstructure has been detected by different etchants.

The volume fractions calculated from images corresponding to etchants No. 1 and No. 2 have more similarities with the amounts reported in different references and papers [22, 23]. It should be noted that use of matrix phase etchants causes overestimation of the γ' precipitates' volume fraction. Salehi et al. [24] have also referred to this issue in their research. When the corrosive etchants of matrix phase are used for nickel-base superalloys, depending on the time of etching and corrosion rate, some of underlying layers of the microstructure may be resolved in the γ' precipitates without any significant change. Therefore, in addition to the surface layer precipitations, subsurface precipitates are also observed during the etching process. Considering the depth of field and focus power of SEM, both surface and subsurface precipitates can be observed and therefore separation and identification of the surface and subsurface γ' precipitates from each other become difficult by using SEM images and total observable precipitates (both surface and subsurface) contribute in measuring the volume fraction of γ' precipitates. This error in the detection of surface precipitates is one of the main reasons for overestimation of γ' precipitates' volume fraction in the samples which are etched by corrosive etchants of the matrix phase. Etching time is also an important factor that, depending on the type of the etchant used, it can be effective in the qualitative and quantitative investigations. Low etching time with the corrosive etchants of γ' precipitates causes γ' particles to retain on the microstructure and makes the error in measuring the size and volume fraction of γ' precipitates. In matrix corrosive etchants, excessive etching time leads to deep etch and reveals the subsurface γ' particles and causes overestimation of γ' precipitates' volume fraction in quantitative measurement by SEM. The morphology and average diameter of the particles are important microstructural characteristics that are investigated in the superalloys. In Table 4, average diameter of the primary γ' precipitates in different microstructures revealed by different etchants are given.

According to Table 4, it is obvious that Etchant type does not have a significant effect on the measurement of γ' particle size. Nevertheless, by comparison of the SEM images in Fig. 4, it can be said that matrix phase corrosive etchants create the perfect embodiment for investigating the superficial morphology of γ' precipitates in superalloys due to development of the three-dimensional space.

3.2 Microstructural Investigation of the Airfoil Section

Figure 6 shows the optical metallography image of the airfoil after long term exposure to high temperature. The blade used in this study has undergone a long period of operation and its microstructure has undergone some

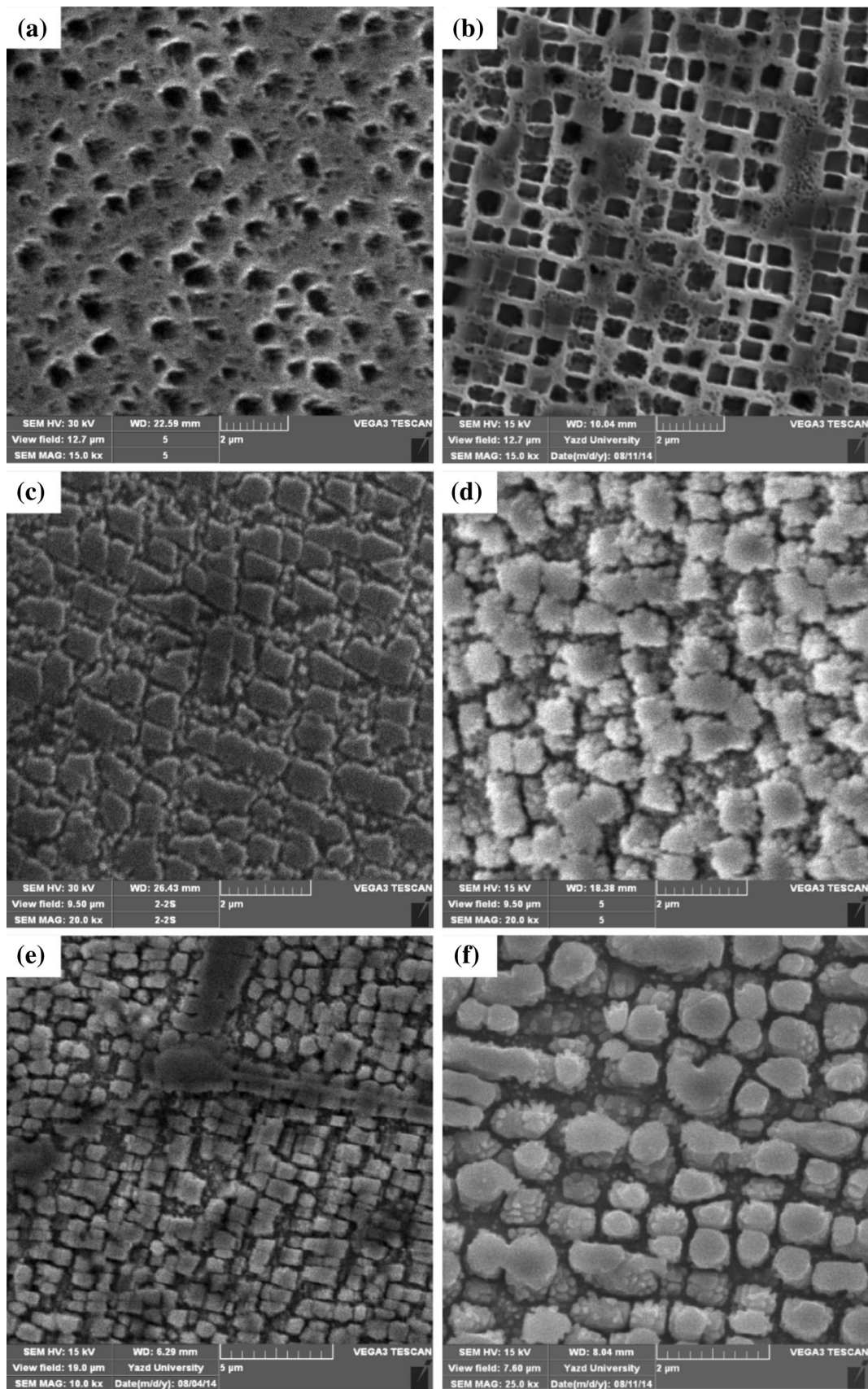


Fig. 4 SEM micrographs of γ' Precipitates in root section, etched by etchant **a** No. 1, **b** No. 2, **c** No. 3, **d** No. 4, **e** No. 5, **f** No. 6

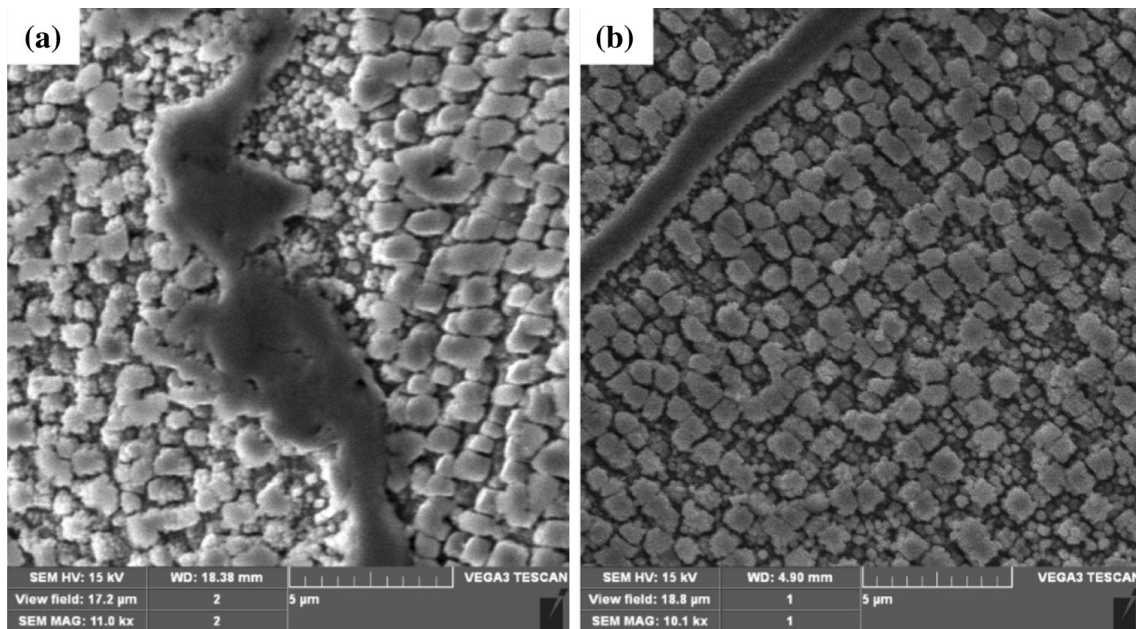


Fig. 5 SEM micrographs of the γ' precipitates' deformation and continuous γ' film on grain boundary in root specimens etched by etchant **a** No. 4, **b** No. 5

Table 3 Volume fractions of the primary γ' calculated in the same samples of root section etched by different etchant

Etchant no.	Volume fraction (%)
1	47 ± 5
2	43 ± 5
5	62 ± 5
6	58 ± 5

Table 4 Average diameter of the primary γ' calculated in the same samples of root section etched by different etchant

Etchant no.	Average diameter (μm)
1	0.78 ± 0.05
2	0.76 ± 0.05
5	0.815 ± 0.05
6	0.8 ± 0.05

changes including coarsening of γ' precipitates and γ' continuous film formation on grain boundary. Since damaging effects of high temperature on the microstructure have micron dimensions, optical microscope images are not suitable tools to visualize these changes. However, the grain boundary carbide particles can be seen in this picture (colored particles in Fig. 6). As mentioned, continuous γ' film on grain boundaries is the most important characteristics of the used blade microstructure. Figure 7 shows SEM images of the grain boundary of the airfoil section etched by different etchant. Figure 7a, b are related to the

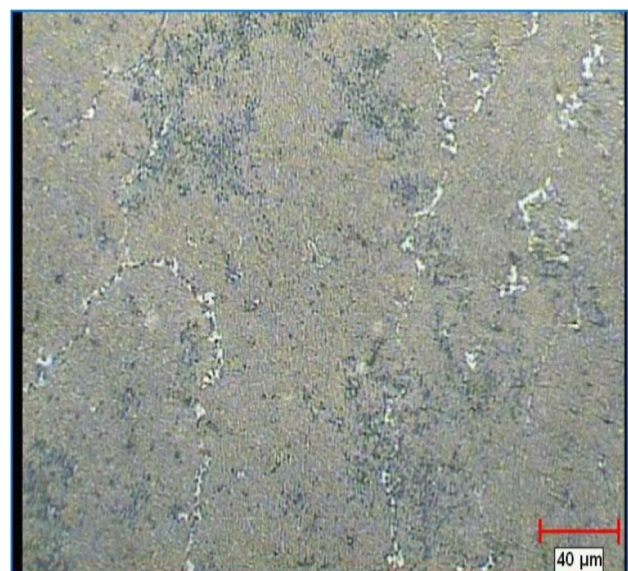


Fig. 6 Optical micrograph of the airfoil specimen after long term services at high temperatures, etched by etchant No. 5

etchants No. 1 and No. 2 that demonstrate microstructure by corrosion of γ' phase. In the airfoil section investigated in this study, due to a long period of operation, γ' precipitate is always available as continuous films of γ' phase formed along the grain boundaries that it is clearly observed in Fig. 7c, d.

A fundamental difference of Fig. 7a, b compared to Fig. 7c, d is that, it is not possible to observe the continuous film of γ' precipitates on grain boundary in Fig. 7a, b due to

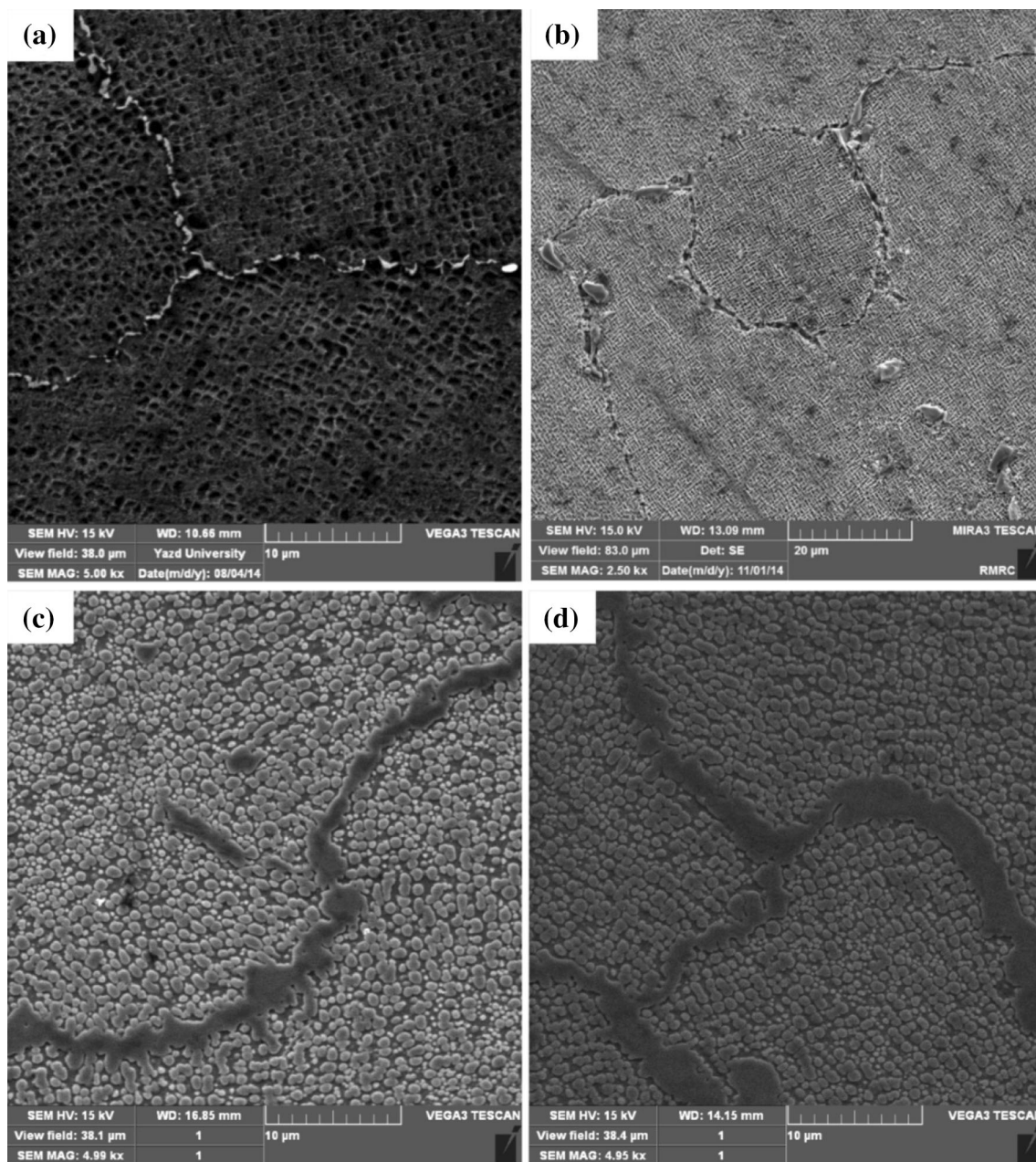


Fig. 7 SEM micrograph of the airfoil section, etched by etchant **a** No. 1, **b** No. 2, **c** No. 4, **d** No. 5

corrosion in γ' phase by etchants No. 1 and No. 2. Figure 8 shows the SEM images of the airfoil sample etched by etchant No. 3. Although the main effect of this etchant is on the matrix and Fig. 8 shows the γ' phase particles clearly, according to Fig. 8, in addition to the matrix, $M_{23}C_6$ carbides in the grain boundaries are also subject to corrosion.

One of the changes that occur during long time use is creation of creep cavities in the grain boundary [25]. Regarding the images observed in this study and comparing this image with images of Fig. 7c, d, it seems that the cavities observed in Fig. 8 are not cavities caused by creep, but they are grain boundary carbides that have been

completely destroyed due to corrosion created by etching process. Because firstly, creep cavities have larger dimensions [26, 27] and Secondly, if these areas are creep cavities, their equivalent should be seen in other samples etched by etchants No. 4 and No. 5 (Fig. 7a, d). Other important changes that occur in the turbine blades due to working at high temperature are MC carbide decompositions. Decomposition of carbides occurs due to the carbon diffusion into the matrix phase and these reactions often continue throughout the life of the alloy and create a transition zone around MC carbide. Carbide reaction in most of the alloys is as Eqs. 1 and 2:

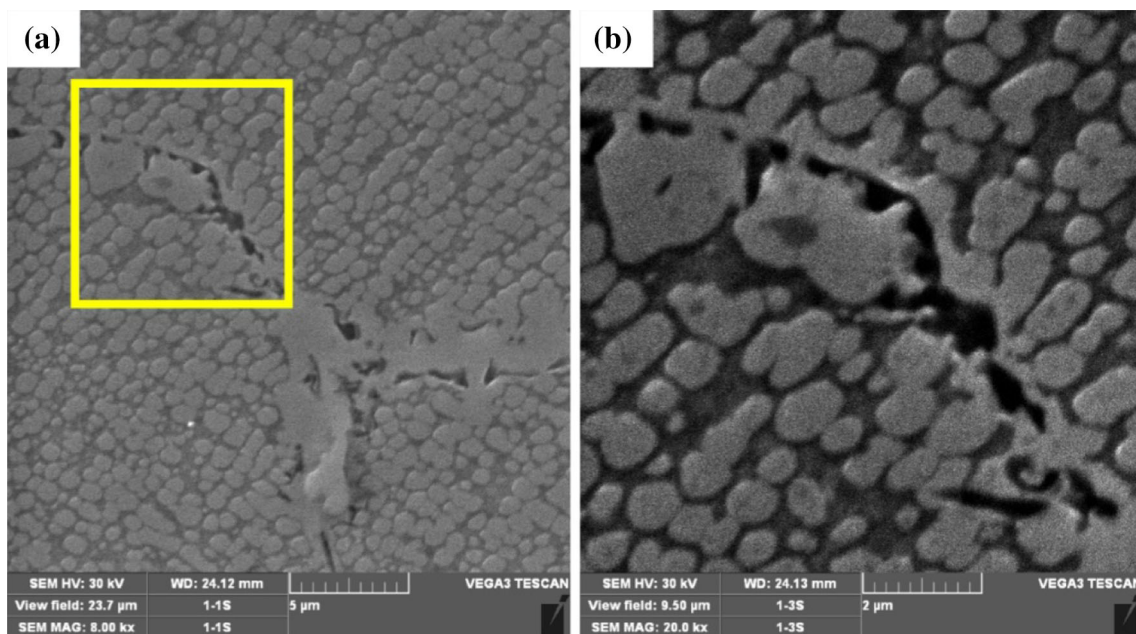


Fig. 8 SEM micrograph of the airfoil section, etched by etchant No. 3, **a** the image of coarsened grain boundary, **b** higher magnification of the area specified in image **a**

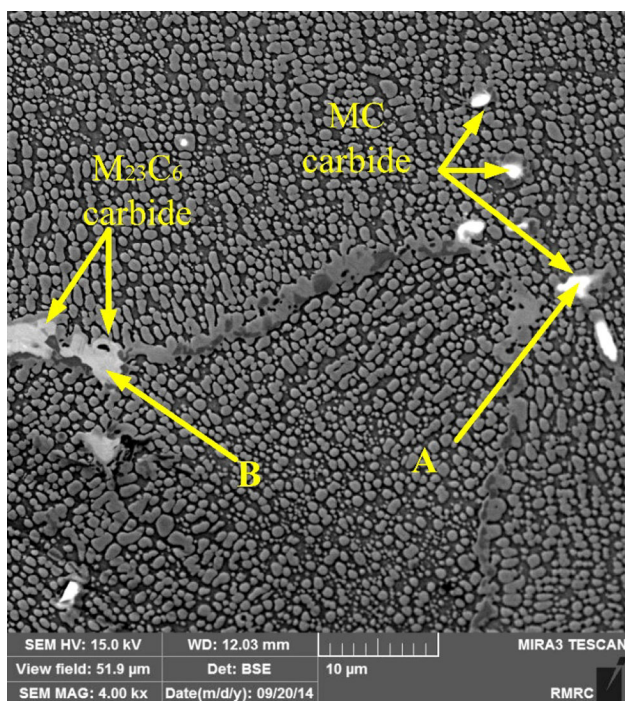
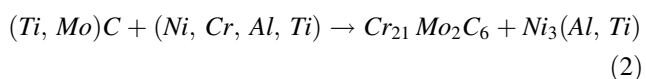


Fig. 9 SEM micrograph of the airfoil etched by etchant No. 5



Regarding the experimental results of microstructural investigations conducted in this study, it has been found

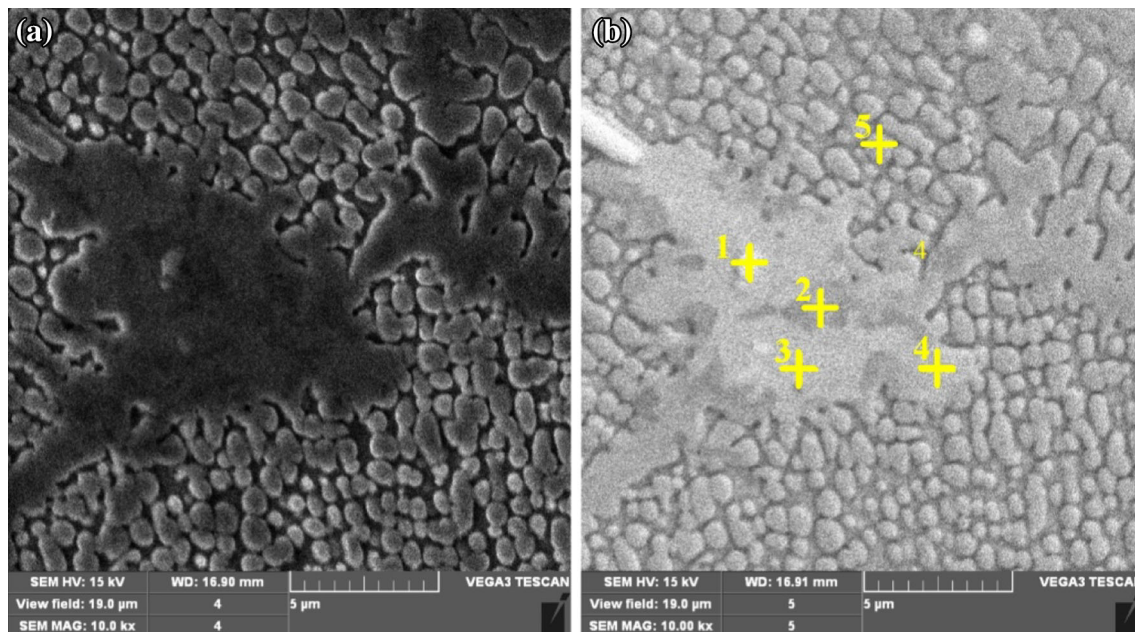
that, among the etchants used, only No.4 and No.5 are able to show the transition zone around decomposed carbides due to a long operation period.

Figure 9 is the image provided by the backscattered electron detector. EDS analysis resulted from A point (MC carbide) and B point ($M_{23}C_6$ carbide) in Fig. 9 are shown in Table 5. As can be seen in Table 5, EDS analysis obtained from MC carbides show relatively higher amounts of Ti, Nb and Ta than $M_{23}C_6$ carbides. Figure 10a, b are SEM images provided by the secondary and the back scatter detector respectively from a decomposed carbide and the results of the EDS points specified in Fig. 10b have been presented in Table 6. In Fig. 10b the basic core of MC carbide is observed with lighter color (point 1). An elemental analysis of the basic core of carbide shows the presence of elements with high atomic mass such as Ti and Ta. It should be noted that decomposition of MC carbides is accompanied with a sharp decline in their size and formation of large amount of $M_{23}C_6$ around them. This reduction of the basic core size of MC carbide and the formation of $M_{23}C_3$ around it, is observed in Fig. 10b.

Replacing the strong carbide former elements such as Ti, Ta and Nb with elements such as Mo and Ni and Cr weakens the atomic bond in the MC carbides and reduces stability of these carbides and this issue leads to the decomposition of MC Carbide and formation of more stable $M_{23}C_6$ carbide around the central core of MC Carbides [28, 29]. In various literatures, chemical reactions related to Carbide decomposition are declared as Eq. (1) [30, 31]. According to the reaction written above, $M_{23}C_6$ is

Table 5 EDS analysis results from marked location in Fig. 9

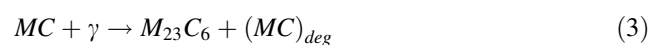
Location	Concentration (wt.%)										
	C	Al	Ti	V	Cr	Co	Ni	Nb	Mo	Ta	W
A	11.4	0	25.71	0	0	0	1.42	9.84	0.88	47.26	2.96
B	19.6	0.54	8.65	0	1.86	4.46	75.89	1.82	2.8	7.80	2.42

**Fig. 10** SEM micrograph of carbide degeneration in the airfoil microstructure etched by etchant No. 4, **a** secondary electrons detector, **b** back scatter electrons detector**Table 6** EDS analysis results for airfoil specimen from marked location in Fig. 10b

Location	Concentration (wt.%)									
	C	Al	Ti	Ta	Mo	Cr	Co	W	Ni	
1	13.9	–	8.0	11.5	–	1.5	4.6	–	61.1	
2	15.9	1.1	3.0	–	3.1	42.5	2.4	4	28.2	
3	16.4	3.7	6.4	–	–	2.1	4.0	–	65.6	
4	8.5	2.4	5.2	–	–	7.9	5.3	1.4	68.8	
5	2.5	4.5	5.4	–	–	5.4	–	–	71.5	

formed in the margin of initial MC and it is expected that adjacent zones include γ' phase. The EDS spectrum in the points around the decomposed Carbide shows significant amounts of carbon and this issue indicates that the region including the analysis points may not be γ' phase. Chemical analysis of the γ' phase particle around the MC Carbide shows this difference. Lvova and Norsworthy [30] in their research have mentioned the formation of a phase except γ' around the MC Carbides. After detailed study of decomposed MC carbides in the used blades of IN738-LC

superalloy, they declared that decomposition reaction of MC carbides while working at high temperature is Eq. 3. In this equation, $(MC)_{deg}$ is a kind of destroyed carbide by a significant reduction in the percentage of carbon.



EDS analysis of the γ' phase and the decomposed area around the MC carbide (Fig. 10 and Table 6) shows the difference in carbon percentage. These results are similar to results obtained by Lvova and Norsworthy [30].

4 Conclusion

- Different etchants used in this research, in order to reveal the microstructure of IN738 LC superalloy can be divided into two groups: First, etchants that affect the γ' phase particles and act with the activation of corrosion mechanisms in this phase. Second, etchants which cause corrosion in the matrix phase.
- Etchants No. 1 and No. 2 are suitable for revealing the segregation of alloying elements, particularly dendrites and dendritic arms and cause the corrosion of γ' phase particles.
- Etchants No. 3 to No. 6 provide an appropriate matrix contrast for investigating the γ' phase morphology and quantitative studies by creating corrosion in the solid solution.
- In order to detect the thickening and continuity of grain boundaries, etchants No. 4 and No. 5 are the most appropriate etchants due to γ' phase precipitation caused by working at high temperatures.
- For the morphological studies and sizing of γ' precipitates by SEM images, using the matrix corrosive etchants are more favorable method due to the corrosion of the matrix phase and creating three-dimensional space.
- In order to calculate the volume fraction of the γ' phase particles, using the corrosive etchants of the matrix phase leads to measurement errors, due to the revealing of subsurface precipitates. Therefore, in such cases, use of the corrosive etchants of the γ' phase is recommended.
- Etchant type has no significant effect on measurement of the primary γ' particles' size.

References

1. Ross E W, and Sims C T, *Superalloy II*, John Wiley & Sons, New York (1987) p 97.
2. Steiner R, *Metals Handbook*, vol. 1, ASM International, Materials Park, OH (1990), p 950.

3. Briant C L, *Mater Manuf Process* **15** (2000) 155.
4. Schafrik R, and Sprague R, *Adv Mater Process* **162** (2004) 27.
5. Liburdi J, Lowden P, Nagy D, De Priamus T R, and Shaw S, *ASME Turbo Expo 2009: Power for Land, Sea, and Air*, p 819.
6. Walston W S, Schaeffer J C, and Murphy W H, *Eight International Symposium of Superalloys*, The Minerals, Metals & Materials Society, Pittsburgh (1996) p 9.
7. Sims C T, and Hagel C W, *The Superalloys-Vital High Temperature Gas Turbine Materials for Aerospace and Industrial Power*, John Wiley & Sons, New York (1972).
8. Ross E W, and Sims C T, *Superalloy I*, John Wiley & Sons, New York (1972).
9. Moshtaghin R S, Asgari S, *Mater Des* **24** (2003) 325.
10. Jayanth C S, Nash P, *Mater Sci Technol* **6** (1990) 405.
11. Ray A K, Singh S R, Swaminathan J, Roy P K, Tiwari Y N, Bose S C, and Ghosh R N, *Mater Sci Eng A* **419** (2006) 225.
12. Hosseini S S, Nategh S, and Ekrami A A, *J Alloys Compd* **512** (2012) 340.
13. Chellman D J, and Ardell A J, *Acta Metall* **22** (1974) 577.
14. Yang J, Zheng Q, Ji M, Sun X, and Hu Z, *Mater Sci Eng* **528** (2011) 1534.
15. Jafari A, Abbasi S M, Rahimi A, Morakabati M, and Seifollahi M, *Assoc Metall Eng Serb* **21** (2015) 167.
16. Liu L, Sommer F, and Fu H Z, *Scripte Metallurgica et Materialia* **30** (1994) 587.
17. Donachie M J, and Donachie S J, *Superalloys—A Technical Guide*, ASM International, Materials Park, OH (2002).
18. Zhao S, Xie X, Smith G D, and Patel S J, *Mater Lett* **58** (2004) 1784.
19. James A, *Mater Sci Technol* **17** (2001) 481.
20. Mazur Z, Luna-Ramirez A, and Juárez-Islas J A, Campos-Amezcuca A, *Eng Fail Anal* **12** (2005) 474.
21. González M A, Martínez D I, Pérez A, and Garza A, *MRS Proc* **1275** (2010) S3.
22. Danis Y, Arvieu C, Lacoste E, Larrouy T, and Quenisset J M, *Mater Des* **31** (2010) 402.
23. Davis J R, *ASM Specialty Handbook: Nickel, Cobalt, and Their Alloys*, ASM International Handbook Committee, Ohio (2000).
24. Salehi R, Samadi A, and Savadkoobi M, *Metallogr Microstruct Anal* **1** (2012) 290.
25. Brown J A, Freer R, and Rowley A T, *J Eng Gas Turbines Power* **123** (2001) 57.
26. Sugui T, Jun X, Xiaoming Z, Benjiang Q, Jianwei L, Lili Y, and Wuxiang W, *Mater Sci Eng A* **528** (2011) 2076.
27. Carter T J, *Eng Fail Anal* **12** (2005) 237.
28. R.A. Stevens, P.E.J. Flewitt, *Mater. Sci. Eng.* **37** (1979) 237-247.
29. Stevens R A, and Flewitt P E J, *Mater Sci Eng* **50** (1981) 271.
30. Lvova E, and Norsworthy D, *J Mater Eng Perform* **10** (2001) 299.
31. Lvova E, *J Mater Eng Perform* **16** (2007) 254.